Dalton Transactions

ROYAL SOCIETY OF CHEMISTRY

FRONTIER

View Article Online
View Journal | View Issue

Cite this: *Dalton Trans.*, 2021, **50**, 3109

2-D spin crossover materials at the nanometric scale: the effects of the size-reduction on the magnetic properties

Vassilis Tangoulis, *[a] Christina D. Polyzou,[a] Patroula Gkolfi,[a] Nikolia Lalioti,[a] Ondrej Malina [b] and Michaela Polaskova[b,c]

Received 25th January 2021,
Accepted 7th February 2021

DOI: 10.1039/d1dt00250c

rsc.li/dalton

Spin Crossover (SCO) particles at the nanometric scale provide an alternative point of view and a new perspective concerning the development of a new generation of spintronic, electronic, photonic and mechanical devices. The coexistence of the SCO phenomenon with the accompanying hysteresis loop enhances the functionality of future devices for storing and processing information. Despite all promising facts, the SCO phenomena are greatly affected by cooperativity issues resulting in a direct relation between the decrease of the size of nanopatricle and the overall decrease of cooperativity towards more gradual spin transitions. This minireview aims to summarise the synthetic techniques for the synthesis of 2-D Fe^{II} SCO particles at the nanometric scale, an underexplored area of research, highlighting the effects of the size-reduction on the magnetic properties of the corresponding nanoparticles and hopefuly showcasing the importance of studying in the context of 2D limit the SCO phenomena.

1. Introduction

The concept of functional nanodevices based on nanoscale Fe^{II} Spin Crossover (SCO) materials appears to be a promising research topic based on the plethora of scientific groups working in this field and the increasing attention in recent years.[1–6] Due to the unique property of SCO materials of undergoing reversible switching between a high spin state (HS) and a low spin state (LS), new spintronic, electronic, photonic, mechanical devices can be fabricated where the SCO materials will be used for storing and processing information and/or for converting different forms of energy in actuators or sensors.[1] Important discoveries intensify the interest for SCO materials, in particular: (i) the coexistence of SCO with hysteresis loop providing the possibility of the memory effect;[7] (ii) SCO transition at room temperature;[8] (iii) the triggering of the spin state using a plethora of external stimuli;[9–11] and (iv) the existence of bistable characteristics in SCO nanoparticles (NPs).[12–16]

However, the interconnection of physical properties and spin state, especially at the nanoscale, remains to be explored and thoroughly studied, since SCO phenomena are greatly affected by cooperativity issues among the SCO centres influencing directly the abruptness of the SCO transition and eventually the width of the hysteresis.[1,12–16] Therefore, experimental and theoretical research is focused on the correlation of the size effect and the first-order phase transition of SCO systems and how the characteristics of the hysteresis are expected to be influenced by the number of molecules forming the nanoparticle. A crucial requirement for successful fabrication of devices is the preservation of the bistability and the cooperativity between the SCO centers during the downsizing experimental protocol.

So far, an extensive amount of studies[1,12–22] refers to the downsizing effects on nanoparticles (NP) of the 1-D iron triazole polymers of the type $[Fe(Htrz)(trz)]^+$ and the 3-D Hofmann polymer $[Fe(pz)Pt(CN)4]\cdot nH_2O$, where Htrz = triazole and pz = pyrazine. The study of these systems revealed a direct relation between the decrease of the particle size and the decrease of cooperativity towards gradual SCO transitions, lower transition temperatures, increase of the residual HS fraction and narrower hysteresis phenomena.

The case of 2-D SCO NPs remains almost unexplored, especially for systems consisting of ultra-thin 2-D nanosheets as building blocks. Given the interest of the scientific community for alternative chemical approaches of graphene and graphene related products, 2-D SCO NPs provide an ideal platform

[a]*Department of Chemistry, University of Patras, 26504 Patras, Greece. E-mail: vtango@upatras.gr*
[b]*Regional Centre of Advanced Technologies and Materials, Czech Advanced Technology and Research Institute, Palacký University, Křížkovského 511/8, Olomouc, 779 00, Czech Republic*
[c]*Department of Experimental Physics, Faculty of Science, Palacký University Olomouc, 17. Listopadu 1192/12, 771 46 Olomouc, Czech Republic*

for further research due to: (i) the highly accessible active sites on the surface; and (ii) the rich synthetic chemistry based on plethora of organic ligands and metal ions. The correlation of the advantages of ultrathin 2-D nanosheets with the downsizing of SCO materials may provide an ideal fabrication protocol for devices with well optimized SCO properties. The present minireview focuses on the 2-D SCO Coordination Polymers (CPs) describing some important nano synthetic methods while in a parallel manner presents the effects of the size-reduction on the magnetic properties of the corresponding nanoparticles (nCPs). More explicitly, the covered nanosynthetic techniques will be: (a) reverse micelle technique, (b) Layer-by-Layer (LBL) method and (c) Liquid Phase Exfoliation (LPE) method.

2. Reverse micelle technique: shape and size effects on 2-D Fe^{II} SCO nanoparticles

The reverse micelle technique has been widely used as an effective method for the synthesis of Fe^{II} SCO particles at the nanometric scale. The first use of this method was reported by Mann and coworkers[23] in an effort to prepare Prussian blue nanoparticles. Although, many reviews until now[1,14,16,24] present the application of this nanosynthetic protocol in the synthesis of 0-D, 1-D and 3-D Fe^{II} SCO polymers, in this minireview our attention is paid exclusively on the limited 2-D Fe^{II} SCO systems.

In 2010 Martinez *et al.*[25] reported for the first time the downsizing effect on 2-D SCO coordination polymer (Fig. 1a) with the formula $[Fe(3\text{-}Fpy)_2M(CN)_4]$ (M^{II} = Ni, Pd^{II}, Pt^{II} and 3-Fpy = 3-fluoropyridine).[26] The resulting fabricated SCO nanocrystals were synthesized by using two water in oil microemulsions with the anionic sodium bis-(2-ethylhexyl)sulfosuccinate (NaAOT) as stabilizer at constant $[H_2O]/[NaAOT]$ ratio. The dimensions of the so called "nanocrystals" were found 400 × 400 × 30 nm as evidenced by TEM microscopy (inset in Fig. 1b). A better quality of nanocrystals was achieved by lowering the temperature reaction at 0 °C which resulted in a narrower size distribution. Fig. 1b shows the magnetic susceptibility measurements for the bulk compound **1** (red solid spheres) and the nanocrystals. It is clear that there is an explicit trend in the decrease of the thermal hysteresis width (from 24 to 10 K) as the size diminishes revealing the dependence of the cooperativity -between SCO centers- on the particle size reduction. A well-defined square shaped hysteresis loop appears for the bulk compound, while for the nanocrystals a gradual hysteresis loop is present due to the large particle-size distribution (olive oil color spheres). Concerning the nanocrystals of the same dimensions but with smaller size distribution a more symmetrical hysteresis loop is revealed (blue color spheres). Furthermore an increase in the residual HS fraction is also present for both cases of nanoparticles. The same trends are also observed for the polymeric Pd^{II} and Pt^{II} analogues. The SCO phenomenon is also accompanied by a color change between the HS state (red) and LS state (yellow). Further decrease of the size of the nanocrystals (70–200 nm) was possible only with the use of polyvinylpyrrolidone (PVP). However, the covering of nanoparticles with the protecting polymer did not result in a hysteretic behavior and instead took place an incomplete and continous second order spin transition.

In 2019 Rubio-Giménez *et al.*[27,28] prepared nanocrystals with the formula $[Fe(py)_2Pt(CN)_4]$[29] (Fig. 2a) in different sizes (41 and 129 nm) and its bulk analogue (46 μm) observing the same trend in their magnetic response (Fig. 2). It is worth mentioning that in this case the nanoparticles were not synthesized by the reverse micelle method but with direct synthesis.

Further investigation of the 2-D system $[Fe(py)_2Ni(CN)_4]$ was made also by Yang *et al.*[30] in an effort to study the dependence of SCO properties on the morphology of the nanostructures. The reverse micelle technique was used in order to successfully prepare ultrathin nanosheets with a thickness less than 10 nm. Two water in oil microemulsions were mixed with the

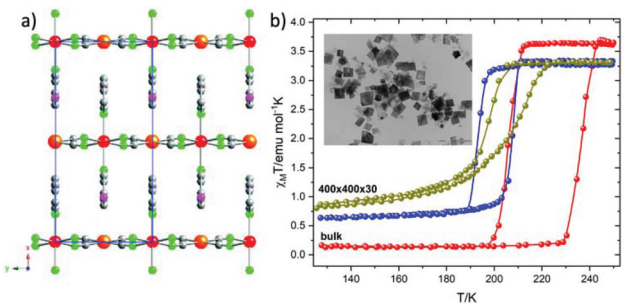

Fig. 1 (a) Packing of the 2D layers of $[Fe(3\text{-}Fpy)_2M(CN)_4]$ (M^{II} = Ni(1), Pd^{II} (2), Pt^{II} (3) compounds along *x*-axis. Atom code: Fe, red; Ni/Pd/Pt, orange; N, green; C, gray; (b) the effect of downsizing of $[Fe(3\text{-}Fpy)_2Ni(CN)_4]$ on the magnetic properties from bulk crystals (red spheres) to nanoplates with dimensions 400 × 400 × 30 nm (oil spheres) and narrower size distribution of the same nanoplates (blue spheres). Adapted from ref. 25 with permission from the American Chemical Society, copyright 2010.

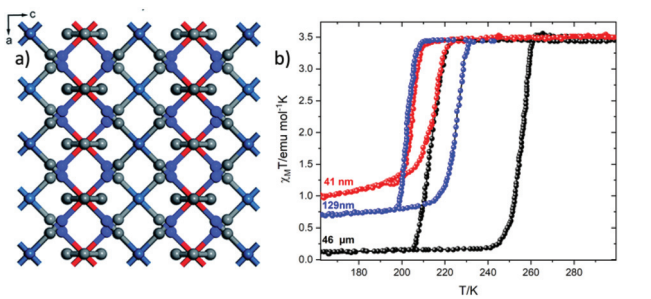

Fig. 2 (a) Grid-like layers of $[Fe(py)_2Ni(CN)_4]$ along the *b* axis; color code: Fe, red; Pt, turquoise; N, blue; C, grey; (b) the effect of downsizing of $[Fe(py)_2Ni(CN)_4]$ on the magnetic susceptibility. Adapted from ref. 28, licensed under CC BY 3.0, published by the Royal Society of Chemistry.

anionic NaAOT as stabilizer and *n*-octane as the oil phase. Slight modifications in the experimental process, such as varying reaction temperature/time and reagent concentration ended up in different nanostructures such as square plate-, cube- and box-like shapes. The magnetic susceptibility measurements revealed that the spin-transition is strongly influenced by the shape of the nanostructures as the hysteresis width decreases in the order of nanoplates (*ca.* 22 K), nanocubes (*ca.* 16 K), nanoboxes (*ca.* 4 K) and nanosheets (*ca.* 2 K). In the case of the two latter examples, the nano-effect is more pronounced accompanied by the weakening of cooperativity and diminishing SCO domain, due to the larger specific surface area. However, size distribution in the case of nanosheets could be an extra factor which might affect the character of spin-transition, adopting a continous shape of the hysteresis with higher than usual T_c.

The latter observation reported also by our group[31] in another example of nanofabrication using the reverse micelle method. The synthesized 2-D SCO nanoparticles with the formula $[Fe^{II}(2\text{-mpz})_2Ni(CN)_4]$ (2-mpz = 2-methylpyrazine) were also synthesized by using two water in oil microemulsions with the NaAOT as stabilizer and *n*-hexane as the oil phase. High Resolution TEM microscopy (Fig. 3a) revealed that the nanoparticles adopt a platelet morphology with distinctive almost square faces between 300 and 600 nm. Fig. 3b shows the magnetic susceptibility measurements for the nanoparticles (blue solid spheres), as well as for the respective bulk material (black solid spheres). Although the bulk material presents a two-step abrupt hysteresis, the downsizing effect on this polymer leads to one-step gradual hysteresis with a much smaller width. This behavior is considered a common trend in 2-D and 3-D coordination polymers when a size reduction is present. Regarding the critical temperatures of the spin-transition for the nanoparticles, these are found to be between the temperature range of the hysteresis width of the bulk material. This behavior is closely related to the polydispersity and large size distribution of the nanoparticles.

Recently our group[32] reported an extensive variable-temperature Raman study of these systems which certified not only the dimensionality of the polymers, but also the spin transition. Micro- and nano-sized samples were compared displaying alterations in their transition curves with the latter ones exhibiting smearing of the sharp transition implying the preservation of HS population in the low-temperature region and the persistence of LS population in the high-temperature region.

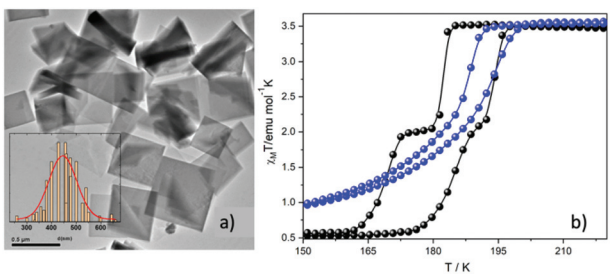

Fig. 3 (a) TEM images of nanoplates of $[Fe^{II}(2\text{-mpz})_2Ni(CN)_4]$ and distribution of their sizes; (b) temperature dependence of the susceptibility data, in the form of $\chi_M T$ for the nanoplates (blue spheres) and the bulk crystal (black spheres). Adapted from ref. 16 with permission from the American Chemical Society, copyright 2019.

3. Layer-by-layer (LBL) method: downsizing from bulk materials to 2-D Fe^{II} SCO thin films

The Layer-by-Layer (LBL) method is known for the fabrication of nanometer-sized coordination polymer thin films. This step-by-step approach was evolved by Mallouk *et al.*[33–35] in order to construct thin films of various CPs even though this method was introduced for the first time around mid 60s'.[36] The LBL method uses structural components and self-assembled monolayer (SAM)-functionalized substrates in liquid phase. Solutions of metal ions and organic ligands are available for the alternately immersion of the substrates accompanied by intermediate washing steps with pure solvent.[37,38] At the end of immersion cycles the final thickness of the film is determined along with all the desired characteristics such as crystallinity, homogeneity and smoothness.

Rubio-Giménez *et al.*[28] studied for the first time the effect of nanostructuration on the spin-transition in crystalline ultrathin films of the 2-D SCO $[Fe(py)_2[Pt(CN)_4]$. The authors optimized the LBL method by creating modifications in the synthetic procedure reported by Kitagawa *et al.*[39,40] and this resulted in the fabrication of controlled thickness films with both higher efficiency and reproducibility. Fig. 4 shows the process of the ultrathin film fabrication on the SAM-functiona-

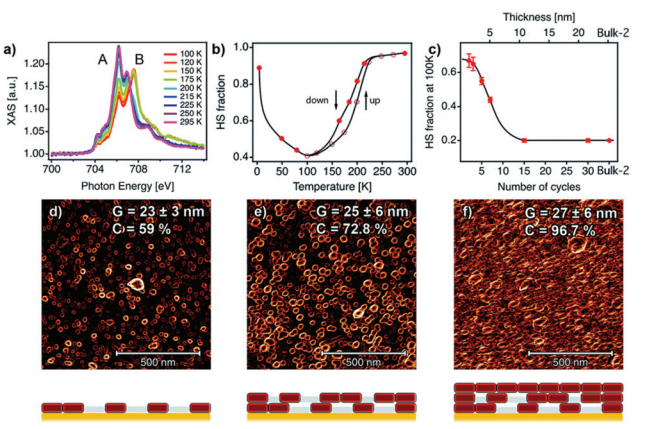

Fig. 4 (a) Temperature dependent XAS spectra for a 7-cycle $[Fe(py)_2Pt(CN)_4]$ thin film; (b) temperature dependent of HS fraction for the 7-cycle film; (c) the dependence of the HS fraction on the number of cycles at 100 K; 1 × 1 μm^2 AFM topography images for a (d) 2-cycles; (e) 5-cycles; (f) 10 cycles thin film. The microstructure of each film is represented below each AFM image. Adapted from ref. 28, licensed under CC BY 3.0 published by the Royal Society of Chemistry.

lized Si/Ti/Au substrate. AFM and X-ray absorption spectroscopy (XAS) were applied for the investigation of the dependence of the SCO bistability on the downsizing effect in films with thickness in a range between 40 and 1 nm (30 to 1 layer). Fig. 4 depicts the SCO behavior of the ultrathin films analysed by XAS data and the correlation with the film microstructure. Raman and magnetic studies were also performed for the same scope but proved to be insufficient due to detection limitations of SCO under 50 nm (ref. 41–43) and 40 nm, respectively. From the XAS study it has been confirmed that the critical value of 10 nm is the marked limit below which the Fe^{II} centers cannot exhibit spin-transition. Downsizing below this critical value has shown a detrimental effect on the properties of the SCO ultrathin films, as the partially segregated crystallites surrounded by a matrix of Fe^{II} centres are blocked in the HS state. When the thickness of the film increases the crystallites coalesce into a homogeneous film resulted in a SCO behavior close to that of the bulk phase.[29] Thus, the dependence of the SCO properties from the thickness cannot be attributed to a size effect, but to interparticle interactions which improve the cooperativity and reduce the residual HS fraction.

Sakaida *et al.*[44] moved on a more meticulous investigation regarding the information which can be extracted from variable temperature Raman Spectroscopy related to the monitoring of SCO in thin films from epitaxial growth. This time LBL method was used for the fabrication of various thickness films of the 2-D SCO $[Fe(py)_2[Pt(CN)_4]$ applying a number of cycles from 20 to 150. Fig. 5 shows the comparison of variable temperature dependent spectra of different thickness films and that of the bulk material. From the graphics is obvious the downsizing effect on the SCO behavior. Starting from the bulk material as the crystallite size decreases the hysteresis is shifted to lower transition temperatures becoming less abrupt. Quite remarkable also is the fact that the thin-film form presents a residual high-spin fraction which is about 20%.

Recently Bartual-Murgui *et al.*[45] reported two new Hofmann-type 2-D SCO polymers with general formulae $\{Fe^{II}(pym)_2[M^{II}(CN)_4]\cdot xH_2O\}_n$ and $\{Fe^{II}(isoq)_2[M^{II}(CN)_4]\}_n$ (pym = pyrimidine, isoq = isoquinoline; M^{II} = Ni^{II}, Pd^{II}, Pt^{II}) synthesized in the bulk form. Their respective Pt counterparts were chosen for the fabrication of thin films through the LBL method. Following the same bottom up approach Rubio-Giménez *et al.*[46] had already reported the fabrication of ultrathin films using the same optimized LBL method in order to study the influence of the different axial nitrogen ligands on the structural flexibility and charge transport properties of the films. However, in this work an intensive structural and magnetic analysis was followed for the crystalline bulk materials showing that both series exhibit strong cooperative thermal induced SCO properties. In the case of films their SCO behavior was investigated through magnetization measurements and then compared with the corresponding samples of the already reported 2-D SCO $[Fe(py)_2[Pt(CN)_4]$ polymer. Although different cycles for the fabrication of the three films were applied -60 for the FepyPt and 90 for FepymPt and FeisoqPt- all showed that it is possible to monitor their SCO behavior. Fig. 6 shows the magnetic susceptibility measurements for FepyPt, FepymPt and FeisoqPt thin films displaying spin-transition. Downsizing of the primitive samples resulted in thin films where the appearance of the hysteresis occurs at lower temperatures than those reported for the corresponding bulk samples. Besides, it is clear that the FepyPt film presents an abrupt and complete hysteresis in comparison to the FepymPt and FeisoqPt films where a remarkable increase of inactive HS Fe^{II} centers is observed. The former exhibits an incomplete and asymmetrical hysteresis, while the latter a complete loss of cooperativity. This is due to the different growth mechanisms-developed for their fabrication- which affect severely their SCO properties. A further confirmation on the effect of SCO properties was given from the thermodynamic parameters extracted from simulation of the magnetization measurements when moving from microcrystalline bulk solids to nanometric thin films.

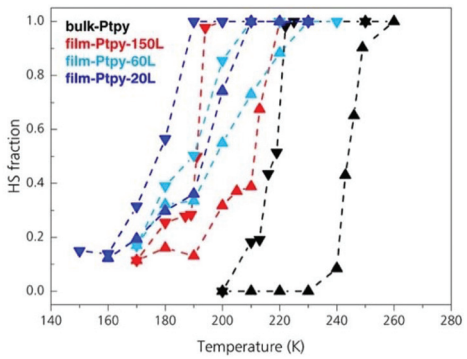

Fig. 5 The effect of downsizing using variable-temperature Raman spectra of bulk-Ptpy (black), film-Ptpy-150L (red), film-Ptpy-60L (cyan), and film-Ptpy-20L (blue). Adapted from ref. 44 with permission from the American Chemical Society, copyright 2019.

4. Liquid phase exfoliation (LPE) method: downsizing from bulk materials to 2-D Fe^{II} SCO nanosheets

Liquid Phase Exfoliation (LPE) is known as a top-down approach[47] for the fabrication of coordination nanosheets, the so called "CONASHs" consisting of both metals centers (inorganic part) and ligands (organic part). These are 2-D molecule-based polymeric materials created from bulk crystalline layered materials, which exhibit intriguing properties and functionalities. For their preparation, ultrasonication is mostly applied in an appropriate solvent where the weakly held together layered structure can be separated. Detection of Tyndall scattering is an initial evaluation of the presence of stable CONASH dispersions. In 2010 Zamora and co-workers[48] reported the first example of the liquid-phase exfoliation of a Metal–Organic Framework (MOF).

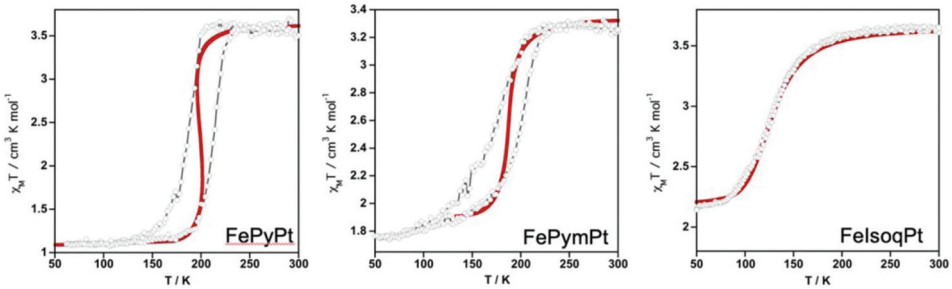

Fig. 6 Temperature dependence of the susceptibility data of the whole mass contained in the thin films and solid red lines present the results of the magnetic simulations. Adapted from ref. 45 with permission from the American Chemical Society, copyright 2020.

Several years later Y.-H. Luo *et al.*[49] reported the ultrasonic force-assisted liquid exfoliation of the bulk van der Waals paramagnetic material $[Fe(1,3\text{-bpp})_2(NCS)_2]_2$ (1,1,3-bpp = 1,3-di(4-pyridyl)propane) into single-layered 2D nanosheets displaying a two-step SCO behavior. The application of the LPE method is considered the first reported in the literature for a 2-D SCO Fe^{II} coordination polymer. Fig. 7a shows the crystallographic description of the rhombic-grid repeating unit of the 2-D sheets. Single-layered 2-D nanosheets have been fabricated from 3-D SCO van der Waals MOF, with thickness of sub-2.0 nm. From the downsizing aspect it is clear that the magnetic response changes from paramagnetic to a two-step SCO behavior while passing from the bulk material to the nanosheets (Fig. 7b). These hybrid systems might be promising for near infrared (NIR) light-triggered molecular switching applications under ambient conditions. In a recent report,[50] three dimensional (3-D) nanoparticles were synthesized by combining the, previously mentioned, 2-D SCO Fe^{II} nanosheets with transition metal ions (Cu^{II}, Ag^{I}). The copper and silver ions were selected as they create strong coordination bonds with the sulfur atoms on both surfaces of the nanosheets. Further modification of the 3-D nanoparticles with loading of Yb^{III}-sensitized hexagonal phase upconversion nanoparticles (UCNPs) was led to an aqueous colloidal suspension with characteristics such as stability, nontoxicity and environmentally friendly behavior. These elements are considered challenging for NIR light-activated molecular conversion under environmental conditions.

Another example of an exfoliated 2-D SCO material using the LPE method is the polymer $[Fe(L_1)_2](ClO_4)_2$ (L_1 = tris(2-(1*H*-tetrazol-1-yl)ethyl)amine) reported by Suarez-Garcia *et al.*[51] In this case delamination of crystals from the 2-D SCO Fe^{II} polymer resulted in the formation of flakes with controlled thicknesses, down to 1–2 nm after 12 hours of sonication. Fig. 8a–c shows the crystallographic description of the 2-D polymer and the packing of the 2-D sheets along the *b*-axis. Various spectroscopic techniques and theoretical study revealed that the flakes retain their chemical identity upon size reduction. Magnetic measurements and temperature dependent absorption spectra outlined that the flakes also preserve the SCO behavior of the bulk state as their size is close to single molecule level (Fig. 8b). From the aspect of their integration in switchable devices, it is interesting to note that the flakes can be stabilized as an aqueous colloidal dispersion for an appreciable time period and then can be deposited on various solid substrates targeting to the formation of thermochromic thin films.

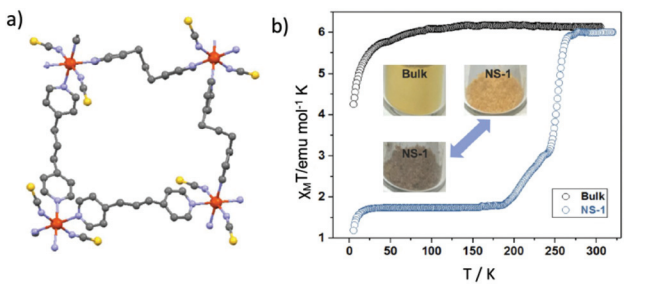

Fig. 7 (a) 2-D sheets are generated by the rhombic-grid unit of (4, 4) Fe(1, 3-bpp)$_2$ color code: Fe, red; N, purple; S yellow; C, grey; (b) temperature dependence of the susceptibility data, in the form of $\chi_M T$, of the exfoliated flakes (blue cycles) and the bulk crystals (black cycles) along with the temperature dependent color changes. Adapted from ref. 49 with permission from the American Chemical Society, copyright 2018.

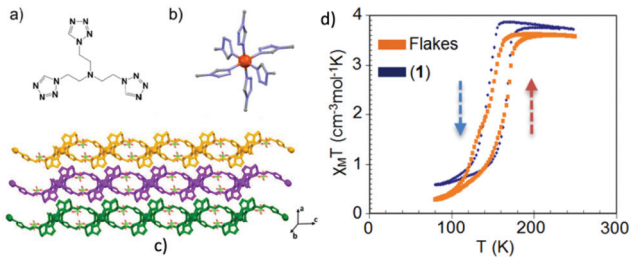

Fig. 8 (a) The tris-tetrazole ligand (L1); (b) the representation of the FeN_6 chromophore in $[Fe(L_1)_2](ClO_4)$ where Fe(II) is shown as a red sphere; (c) packing of the 2D sheets along the *b*-axis; (d) temperature dependence of the susceptibility data, in the form of $\chi_M T$, of the exfoliated flakes (orange) and the crystals (blue) confirming the spin transition phenomenon. Adapted from ref. 50 with permission from the American Chemical Society, copyright 2018.

5. Conclusions

This minireview has highlighted the most important synthetic methodologies for obtaining 2-D Fe^{II} SCO particles in the nanometric scale and their SCO magnetic behavior. It is clear that the database is still in its infancy and new 2-D nanomaterials need to be synthesized to shed light in fundamental questions related to the influence of downsizing at the nanoscale and the so- called 2-D limit. From the magnetic findings so far, it is clear that even for the 2-D SCO NPs the hysteresis property is strongly affected by cooperativity issues when the size of the nanoparticle is decreased. This result is in agreement with the magnetic behavior of the 3-D SCO NPs. Interestingly the bistable behavior is retained in the cases of 2-D SCO thin films for specific ranges of the film thickness denoting the non-existence of any size reduction effects for these ranges and underlying the fact that specific limitations may exist towards the fabrication of ultra-thin films. In a parallel manner the LPE processing of 2-D SCO materials towards atomically thin nano-sheets, retaining their hysteretic SCO character seems to be another promising route towards a new generation of SCO hybrid devices.

We sincerely hope that the pioneering work of the researchers in the area of 2-D SCO nanomaterials become an inspiration pole for the scientific community to envisage their technological potential.

Conflicts of interest

There are no conflicts to declare.

Acknowledgements

C. D. P. acknowledges the State Scholarships Foundation (IKY). This research is co-financed by Greece and the European Union (European Social Fund [ESF]) through the Operational Programme "Human Resources Development, Education and Lifelong Learning" in the context of the project "Reinforcement of Postdoctoral Researchers-2nd Cycle" (MIS-5033021), implemented by the State Scholarships Foundation (IKY).

P. G. acknowledges the financial support by "K. Karatheodori" 2017 research grant (no. 80623) of the University of Patras.

The authors acknowledge the assistance provided by the Research Infrastructure NanoEnviCz, supported by the Ministry of Education, Youth and Sports of the Czech Republic under Project No. LM2018124. The work was also supported by the ERDF/ESF project "Nano4Future" Development of pre-applied research in nanotechnology and biotechnology (no. CZ.02.1.01/0.0/0.0/17_048/0007323).

References

1 G. Molnár, S. Rat, L. Salmon, W. Nicolazzi and A. Bousseksou, *Adv. Mater.*, 2018, **30**, 17003862.
2 J. F. Létard, P. Guionneau, L. Goux-Capes, P. Gütlich and H. A. Goodwin, *Spin Crossover Transit. Met. Compd. III*, 2004, vol. 235, pp. 221–249.
3 C. M. Jureschi, J. Linares, A. Boulmaali, P. Dahoo, A. Rotaru and Y. Garcia, *Sensors*, 2016, **16**, 187.
4 C. Lefter, V. Davesne, L. Salmon, G. Molnár, P. Demont, A. Rotaru and A. Bousseksou, *Magnetochemistry*, 2016, **2**, 18.
5 K. S. Kumar and M. Ruben, *Coord. Chem. Rev.*, 2017, **346**, 176–205.
6 M. D. Manrique-Juárez, S. Rat, L. Salmon, G. Molnár, C. M. Quintero, L. Nicu, H. J. Shepherd and A. Bousseksou, *Coord. Chem. Rev.*, 2016, **308**, 395–408.
7 O. Kahn and C. J. Martinez, *Science*, 1998, **279**, 44–48.
8 S. Cobo, D. Ostrovskii, S. Bonhommeau, L. Vendier, G. Molnár, L. Salmon, K. Tanaka and A. Bousseksou, *J. Am. Chem. Soc.*, 2008, **130**, 9019–9024.
9 A. Bousseksou, F. Varret, M. Goiran, K. Boukheddaden and J. P. Tuchagues, *Spin Crossover Transit. Met. Compd. III*, 2004, vol. 235, pp. 65–84.
10 A. Hauser, Spin Crossover Transit, *Met. Compd. II*, 2004, **233**, 155–198.
11 V. Ksenofontov, A. B. Gaspar and P. Gütlich, *Spin Crossover Transit. Met. Compd. III*, 2004, vol. 235, pp. 23–64.
12 H. J. Shepherd, G. Molnár, W. Nicolazzi, L. Salmon and A. Bousseksou, *Eur. J. Inorg. Chem.*, 2013, 653–661.
13 M. Mikolasek, G. Félix, W. Nicolazzi, G. Molnár, L. Salmon and A. Bousseksou, *New J. Chem.*, 2014, **38**, 1834–1839.
14 L. Salmon and L. Catala, *C. R. Chim.*, 2018, **21**, 1230–1269.
15 T. Mallah and M. Cavallini, *C. R. Chim.*, 2018, **21**, 1270–1286.
16 C. D. Polyzou and V. Tangoulis, *J. Coord. Chem.*, 2019, **72**, 389–418.
17 I. Boldog, A. B. Gaspar, V. Martínez, P. Pardo-Ibañez, V. Ksenofontov, A. Bhattacharjee, P. Gütlich and J. A. Real, *Angew. Chem., Int. Ed.*, 2008, **47**, 6433–6437.
18 F. Volatron, L. Catala, E. Rivière, A. Gloter, O. Stéphan and T. Mallah, *Inorg. Chem.*, 2008, **47**, 6584–6586.
19 J. Larionova, L. Salmon, Y. Guari, A. Tokarev, K. Molvinger, G. Molnár and A. Bousseksou, *Angew. Chem., Int. Ed.*, 2008, **47**, 8236–8240.
20 H. Peng, S. Tricard, G. Félix, G. Molnár, W. Nicolazzi, L. Salmon and A. Bousseksou, *Angew. Chem., Int. Ed.*, 2014, **53**, 10894–10898.
21 J. R. Galán-Mascarós, E. Coronado, A. Forment-Aliaga, M. Monrabal-Capilla, E. Pinilla-Cienfuegos and M. Ceolin, *Inorg. Chem.*, 2010, **49**, 5706–5714.
22 E. Coronado, J. R. Galán-Mascarós, M. Monrabal-Capilla, J. García-Martínez and P. Pardo-Ibáñez, *Adv. Mater.*, 2007, **19**, 1359–1361.
23 S. Vaucher, M. Li and S. Mann, *Angew. Chem., Int. Ed.*, 2000, **39**, 1793–1796.
24 K. Otsubo, T. Haraguchi and H. Kitagawa, *Coord. Chem. Rev.*, 2017, **346**, 123–138.

25 V. Martinez, I. Boldog, A. B. Gaspar, V. Ksenofontov, A. Bhattacharjee, P. Gutlich and J. A. Real, *Chem. Mater.*, 2010, **22**, 4271–4281.
26 V. Martinez, A. B. Gaspar, M. C. Muñoz, G. V. Bukin, G. Levchencko and J. A. Real, *Chem. – Eur. J.*, 2009, **15**, 10960–10971.
27 V. Rubio-Giménez, S. Tatay and C. Martí-Gastaldo, *Chem. Soc. Rev.*, 2020, **49**, 5601–5638.
28 V. Rubio-Giménez, C. Bartual-Murgui, M. Galbiati, A. Núñez-López, J. Castells-Gil, B. Quinard, P. Seneor, E. Otero, P. Ohresser, A. Cantarero, E. Coronado, J. A. Real, R. Mattana, S. Tatay and C. Martí-Gastaldo, *Chem. Sci.*, 2019, **10**, 4038–4047.
29 V. Niel, J. M. Martinez-Agudo, M. C. Muñoz, A. B. Gaspar and J. A. Real, *Inorg. Chem.*, 2001, **40**, 3838–3839.
30 Y. Yang, X. Shen, H. Zhou, L. Lang, G. Zhu and Z. Ji, *J. Magn. Magn. Mater.*, 2020, **496**, 165938.
31 C. D. Polyzou, O. Malina, J. Tuček, R. Zbořil, N. Panagiotou, A. J. Tasiopoulos, N. Boukos, J. Parthenios, A. N. Kalarakis and V. Tangoulis, *Inorg. Chem.*, 2019, **58**, 13733–13736.
32 Z. G. Lada, K. S. Andrikopoulos, C. D. Polyzou, V. Tangoulis and G. A. Voyiatzis, *J. Raman Spectrosc.*, 2020, 1–11.
33 H. Lee, L. J. Kepley, H. G. Hong, S. Akhter and T. E. Mallouk, *J. Phys. Chem.*, 1988, **92**, 2597–2601.
34 C. M. Bell, S. W. Keller, V. M. Lynch and T. E. Mallouk, *Mater. Chem. Phys.*, 1993, **35**, 225–232.
35 H. C. Yang, K. Aoki, H. G. Hong, D. D. Sackett, M. F. Arendt, S. L. Yau, C. M. Bell and T. E. Mallouk, *J. Am. Chem. Soc.*, 1993, **115**, 11855–11862.
36 J. J. Kirkland, *Anal. Chem.*, 1965, **37**, 1458–1461.
37 D. Zacher, O. Shekhah, C. Woll and R. A. Fischer, *Chem. Soc. Rev.*, 2009, **38**, 1418–1429.
38 O. Shekhah, J. Liu, R. A. Fischer and Ch. Woll, *Chem. Soc. Rev.*, 2011, **40**, 1081–1106.
39 S. Sakaida, K. Otsubo, O. Sakata, C. Song, A. Fujiwara, M. Takata and H. Kitagawa, *Nat. Chem.*, 2016, **8**, 377–383.
40 S. Sakaida, T. Haraguchi, K. Otsubo, O. Sakata, A. Fujiwara and H. Kitagawa, *Inorg. Chem.*, 2017, **56**, 7606–7609.
41 C. Bartual-Murgui, A. Akou, L. Salmon, G. Molnár, C. Thibault, J. A. Real and A. Bousseksou, *Small*, 2011, **7**, 3385–3391.
42 G. Agustí, S. Cobo, A. B. Gaspar, G. Molnár, N. O. Moussa, P. A. Szilágyi, V. Pálfi, C. Vieu, M. C. Muñoz, J. A. Real and A. Bousseksou, *Chem. Mater.*, 2008, **20**, 6721–6732.
43 I. A. Gural'skiy, C. Quintero, K. Abdul-Kader, M. Lopes, C. Bartual-Murgui, L. Salmon, G. Molnár, A. Bousseksou, P. Zhao and D. Astruc, *J. Nanophotonics*, 2012, **6**, 063517.
44 S. Sakaida, K. Otsubo, M. Maesato and H. Kitagawa, *Inorg. Chem.*, 2020, **59**, 16819–16823.
45 C. Bartual-Murgui, V. Rubio-Giménez, M. Meneses-Sánchez, F. J. Valverde-Muñoz, S. Tatay, C. Marti-Gastaldo, M. C. Muñoz and J. A. Real, *ACS Appl. Mater. Interfaces*, 2020, **12**, 29461–29472.
46 V. Rubio-Giménez, G. Escorcia-Ariza, C. Bartual-Murgui, C. Sternemann, M. Galbiati, J. Castells-Gil, J. A. Real, S. Tatay and C. Martí-Gastaldo, *Chem. Mater.*, 2019, **31**, 7277–7287.
47 R. Sakamoto, K. Takada, T. Pal, H. Maeda, T. Kambe and H. Nishihara, *Chem. Commun.*, 2017, **53**, 5781–5801.
48 P. Amo-Ochoa, L. Welte, R. Gonzalez-Prieto, P. J. Sanz Miguel, C. J. Gomez-Garcia, E. Mateo-Marti, S. Delgado, J. Gomez-Herrero and F. Zamora, *Chem. Commun.*, 2010, **46**, 3262–3264.
49 Y. H. Luo, C. Chen, D. L. Hong, X. T. He, J. W. Wang and B. W. Sun, *J. Phys. Chem. Lett.*, 2018, **9**, 2158–2163.
50 J.-Y. Wang, Y.-H. Luo, F.-H. Xing, X.-W. Jin, L.-H. Guo, L.-H. Zhai, L. Zhang, W.-X. Fang and B. W. Sun, *ACS Appl. Mater. Interfaces*, 2020, **12**, 15573–15578.
51 S. Suarez-Garcia, N. N. Adarsh, G. Molnar, A. Bousseksou, Y. Garcia, M. M. Dîrtu, J. Saiz-Poseu, R. Robles, P. Ordejon and D. Ruiz-Molina, *ACS Appl. Nano Mater.*, 2018, **6**, 2662–2668.